2026 IEEE International Conference on Robotics and Automation (ICRA 2026)
June 1-5, 2026. Vienna, Austria

Time-Optimal Trajectory Planning and Model Predictive Control of Morphing Quadrotors

Qiuyu Wang, Na Zhao†, Chaojun Qin, Xiyu Ke, Yudong Luo, and Yantao Shen

***Abstract*— Morphing quadrotors offer enhanced maneuverability and adaptability in confined spaces, while their structural variations pose challenges to trajectory planning and control. This paper presents a time-optimal trajectory planning and model predictive control framework for the morphing quadrotor. The trajectory generator computes time-optimal trajectories by dynamically adjusting arm lengths, allowing the quadrotor to traverse waypoints as quickly as possible while satisfying constraints. The generated trajectory is then fed into the designed dual-loop model predictive control architecture to achieve autonomous flight, in which the outer loop tracks the desired trajectory and the inner loop synchronously regulates attitude and the morphing quadrotor's arm length. Experimental validation demonstrates that the proposed framework achieves high-precision trajectory tracking, robust dynamic response, and superior adaptability in confined environments.**

I. Introduction

Due to the control flexibility, vertical take-off and landing capability, high efficiency, and low operating cost, quadrotors have been widely deployed in aerial inspections, logistics, and agriculture to reduce personnel risks, improve mission efficiency, and accelerate the advancement of intelligent control and autonomous flight [1]. However, conventional quadrotors have limited adaptability in cluttered or restricted environments, such as collapsed buildings, pipelines, and dense forests, as their rigid structures make it difficult to navigate through confined and irregular spaces, resulting in degraded mission performance or even mission interruption. To address these challenges, the morphing quadrotor has emerged, which can match environmental constraints through structural transformations such as arm folding and rotor redirection [2]. Nevertheless, the additional actuation components of the morphing mechanism and the complex aerodynamic characteristics lead to high energy consumption, and the limited capacity of the onboard battery further compresses the effective mission time [3].Considering these time limitations, time-optimal trajectory planning becomes crucial, as minimizing task duration not only enhances efficiency but also reduces energy consumption and prolongs battery life.

*This work was supported by the National Natural Science Foundation of China under Grant 52305009 and the Fundamental Research Funds for the Central Universities under Grant 3132025271.

Qiuyu Wang, Na Zhao†, Chaojun Qin, and Yudong Luo are with the Department of Computer Science and Technology, Dalian Maritime University, Dalian, Liaoning, 116026 China. Xiyu Ke is with the Department of Electrical and Computer Engineering, Rutgers, The State University of New Jersey, Piscataway, NJ 08854, USA. Yantao Shen is with the Department of Electrical and Biomedical Engineering, University of Nevada, Reno, NV 89557 USA. Corresponding author†. Email: *zna@dlmu.edu.cn*

Existing time-optimal trajectory planning methods for quadrotors can be broadly classified into two mainstream approaches: sampling-based and polynomial-based approaches. For the first category, a recent study [4] proposes the Complementary Progress Constraint (CPC) method, which jointly optimizes trajectories and time allocation for time-optimal performance. However, the resulting problem is highly non-convex, computationally intensive, and reliant on complex solvers. Another approach [5] formulates a real-time optimization framework that integrates path tracking and time allocation by adaptively adjusting sampling points to maximize progress and reduce contouring errors. In addition, the segmented time-optimal method [6] simplifies the optimization by dividing the trajectory into individual sampling intervals and preallocated waypoint nodes. Polynomial-based methods exhibit notable advantages such as smooth trajectory generation, effective boundary condition handling, and low computational cost. A representative example is the widely adopted approach to generating the minimum snap trajectory [7], [8], which minimizes the fourth derivative of position and the second derivative of yaw to ensure control feasibility through input-derivative relationships. However, high-degree polynomials and multiple constraints significantly increase the complexity of optimization. To address this issue, a Time-Optimal Gate-Traversing (TOGT) method [9] is presented for drone racing, which considers geometric constraints of gates with diverse shapes and sizes. Additionally, the research in [10] focuses on polynomial trajectory planning, particularly the use of fourth-order polynomials to minimize the trajectory snap. The work in [11] introduces an AOS method for constructing long-distance trajectories with minimal polynomial segments by analyzing thrust–angular velocity switching patterns in quadrotor maneuvers. Despite significant progress in time-optimal trajectory generation for conventional quadrotors using existing trajectory planning methods, their core assumptions still remain rooted in fixed-structure quadrotors and neglect the specific characteristics of morphing quadrotors.

In contrast, control frameworks for morphing quadrotors have been more thoroughly investigated, with various approaches developed to exploit their structural adaptability. A novel morphing quadrotor [12] based on cascade PID can adjust its size via folding structures to dynamically adapt to confined spaces. A quadrotor with real-time arm adjustment [13] enables navigation in confined environments and leverages model predictive control for precise trajectory tracking. A retractable quadrotor with a ring-shaped structure enables synchronized morphing via a single actuator

[14], while preserving central space for aerial grasping, and employs a PID-based controller to ensure flight stability during morphing and manipulation. Inspired by an eagle's claw, the biomimetic morphing quadrotor [15] adopts a central servomotor to drive a closed-loop multi-link frame, which enables the vertical arm folding for dynamic in-flight grasping, and implements adaptive sliding-mode control with an admittance filter. An adaptive controller [16] can handle configuration changes and uncertainties in foldable quadrotors using a switched-system and Lyapunov-based design. There are still some limitations in existing morphing quadrotor control frameworks. The works rely on classical PID or cascaded controllers that generally lack robustness against aggressive morphing-induced dynamics or significant configuration changes. Moreover, although adaptive strategies offer improved performance, they typically require accurate modeling, and research specifically addressing real-time dynamic morphing remains limited.

To address the above limitations and enhance the flight efficiency of morphing quadrotors in complex environments, we propose a framework that integrates morphing strategies with both time-optimal path planning and model predictive control (MPC) based dynamic control design. At the planning layer, a time-optimal morphing-aware trajectory method is developed that explicitly incorporates arm-length dynamics, enabling efficient waypoint traversal and minimizing overall flight time. At the control layer, we design a structure-adaptive dual-loop MPC controller that accounts for the quadrotor's time-varying morphology. Furthermore, by leveraging the system's differential flatness property, we simplify the representation of states and inputs, facilitating the integration of planning and control. The main contributions are as follows: i) The increase in power consumption caused by morphing reduces the effective operating time. This is the first attempt to design a time-optimal path planning method for a morphing quadrotor. ii) A full-degree-of-freedom (DOF) dual-loop MPC controller designed to cope with morphing-induced dynamic disturbances in real time, achieving precise trajectory tracking and stability during rapid configuration changes.

The structure of this paper is as follows. Section II describes the system dynamics and the augmented MPC framework for the morphing quadrotor. Section III presents a time-optimal trajectory generation method that accounts for morphological changes. Section IV provides experimental evaluations, including comparative studies, multi-stage radius-transition trajectory generation, and trajectory-tracking performance assessments. Section V concludes the work.

II. Dynamic Modeling and Controller Design

In this section, we design a control framework for a morphing quadrotor that features a dual-loop control strategy integrated with adaptive arm-length adjustment. An overview of the control scheme is illustrated in Fig. 1(a). The arm length ℓ along the trajectory generated in Section III is used to compute the servo angles. Once the position reference

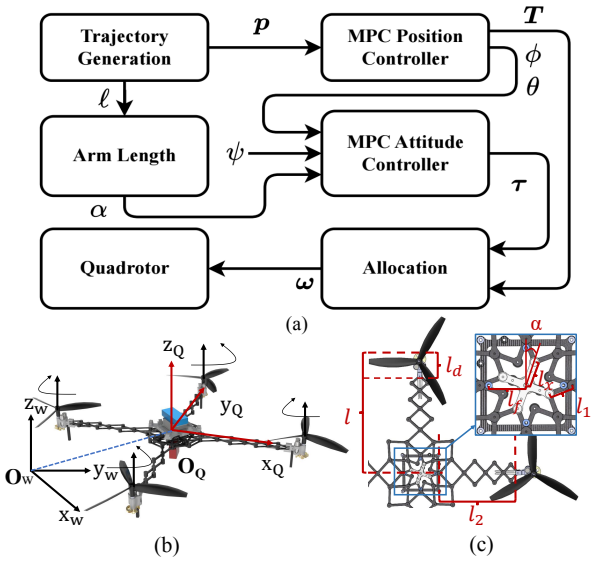

Fig. 1. (a) Overview of control scheme of a morphing quadrotor, (b) the coordinate system, and (c) detailed structure of the morphing arm.

p along the trajectory is obtained, it is fed into the outer loop MPC position controller, which outputs the total thrust T and the desired attitude angles ϕ and θ required by the inner loop MPC attitude controller. The inner loop controller, together with the predefined yaw angle ψ and the servo angles, generates the required control torques τ. Finally, a control allocation module converts τ and T into rotor speed ω, which actuates the morphing quadrotor to execute the corresponding motions and achieve precise trajectory tracking.

A. Quadrotor Dynamics

To clearly describe the position of the morphing quadrotor [12], [17], we denote the world coordinate system as $\mathcal{W} = o_{\mathcal{W}} x_{\mathcal{W}} y_{\mathcal{W}} z_{\mathcal{W}}$ and the body coordinate system as $\mathcal{Q} = o_{\mathcal{Q}} x_{\mathcal{Q}} y_{\mathcal{Q}} z_{\mathcal{Q}}$, as shown in the Fig. 1(b). The center of mass of the quadrotor coincides with the origin of the body coordinate system, denoted as $o_{\mathcal{Q}}$. The state of the quadrotor is defined as $x = \left[p, \Theta, v, \omega, \ell\right]^T$. Specifically, $p = \left[x, y, z\right]^T$ represents the position vector of the quadrotor along the x, y and z axes expressed in $\mathcal{W}$, $\Theta = \left[\phi, \theta, \psi\right]^T$ denotes the attitude vector of the quadrotor, v is the velocity vector in $\mathcal{W}$, and $\omega = \left[p, q, r\right]^T$ represents the angular velocity in the body coordinate system $\mathcal{Q}$. The dynamic expression of the quadrotor is as follows

$$\ddot{p} = \dot{v} = a, \tag{1a}$$

$$ma = -mge + RF_T, \tag{1b}$$

$$J\dot{\omega} = \tau - \omega \times J\omega, \tag{1c}$$

where a is the acceleration in $\mathcal{W}$, m is the mass of the quadrotor, g is the gravitational acceleration, $e = [0 \quad 0 \quad 1]^T$, $F_T = [0 \quad 0 \quad T]^T$, and $J = diag(J_{xx}, J_{yy}, J_{zz})$ is the moment of inertia. R denotes the rotation matrix from $\mathcal{Q}$ to $\mathcal{W}$ with $R = [c\theta c\psi \quad c\psi s\theta s\phi - s\psi c\phi \quad c\psi s\theta c\phi + s\psi s\phi; c\theta s\psi \quad s\psi s\theta s\phi + c\psi c\phi \quad s\psi s\theta c\phi -$

$c\psi s\phi; -s\theta \quad s\phi c\theta \quad c\phi c\theta]$, where cx and sx denote $\cos x$ and $\sin x$, respectively.

Suppose that ψ is small, (1b) can be rewrite as $ma = -mge + R_{new}u_1$ with $R_{new} = [0\ mg\ 0; -mg\ 0\ 0; 0\ 0\ 1]^T$ and $u_1 = [\phi\ \ \theta\ \ T]^T$. For (1c), we can derive $\dot{\Theta} = \widetilde{R}\omega$, where $\widetilde{R} = [1\ 0\ 0; s\phi t\theta\ \ c\phi\ \ s\phi/c\theta; c\phi t\theta\ \ -s\phi\ \ c\phi/c\theta]^T$ with $tx = \tan x$. By applying the small-angle approximation, the singularity at $\cos\theta = 0$ is avoided, and sine terms are neglected. Consequently, the angular velocity can be directly approximated by the Euler angle rates $[\dot{\phi}\ \ \dot{\theta}\ \ \dot{\psi}]^T = [p\ q\ r]^T$ which means $\dot{\Theta} \approx \omega$.

The torque vector is denoted as $u_2 = \tau = [\tau_1\ \tau_2\ \tau_3]^T$, representing the moments generated by the propellers about the body-fixed axes. The mapping from motor angular velocities to torque is given by

$$\begin{bmatrix} \tau_1 \\ \tau_2 \\ \tau_3 \end{bmatrix} = \begin{bmatrix} 0 & k_T\ell & 0 & -k_T\ell \\ -k_T\ell & 0 & k_T\ell & 0 \\ k_M & -k_M & k_M & -k_M \end{bmatrix} \begin{bmatrix} \omega_1^2 \\ \omega_2^2 \\ \omega_3^2 \\ \omega_4^2 \end{bmatrix} \tag{2}$$

where k_T is the thrust coefficient, k_M is the moment coefficient, $\omega_{j\in[1,2,3,4]}$ denotes the motor speeds, and ℓ is the time-varying arm length of the morphing quadrotor, whose value will be determined later. Then, we can linearize (1c) around the operating point as

$$[\ddot{\phi} \quad \ddot{\theta} \quad \ddot{\psi}]^T = \left[\tau_1/\hat{J}_{xx} \quad \tau_2/\hat{J}_{yy} \quad \tau_3/\hat{J}_{zz}\right]^T \tag{3}$$

where the symbols with hats denote the estimated values of the corresponding variables.

B. Identification of Arm Length Dynamics

Based on the morphing quadrotor design [18], the arm length ℓ is actuated by a servo motor, with the servo angle α as input. From the geometry in Fig. 1(c), the intermediate length is $\ell_1 = \sqrt{(\ell_x \sin\alpha)^2 + (\ell_f - \ell_x \cos\alpha)^2}$, leading to $\ell = \ell_d + \ell_p + \ell_f - \ell_1$, where $\ell_p = \ell_1 + \ell_2$ is measurable, and ℓ_d, ℓ_x, and ℓ_f are constants. The mapping from α to ℓ is approximated as

$$\ddot{\ell}(\alpha) = a\dot{\ell}(\alpha) + b\ell(\alpha) + c\alpha \tag{4}$$

where a, b, and c are identified constants.

C. Augmented Model Predictive Control

Building on [19], we develop a full-DOF MPC that accommodates the varying inertial properties of the morphing quadrotor in the following form of state-space equation.

$$\begin{aligned} \underbrace{\begin{bmatrix} \Delta x(k+1) \\ y(k+1) \end{bmatrix}}_{x(k+1)} &= \underbrace{\begin{bmatrix} A_0 & O_{p_y\times n_x}^T \\ C_0A_0 & E_{p_y\times p_y} \end{bmatrix}}_{A} \underbrace{\begin{bmatrix} \Delta x(k) \\ y(k) \end{bmatrix}}_{x(k)} + \underbrace{\begin{bmatrix} B_0 \\ C_0B_0 \end{bmatrix}}_{B} \Delta u(k) \\ y(k) &= \underbrace{\begin{bmatrix} O_{p_y\times n_x} & E_{p_y\times p_y} \end{bmatrix}}_{C} \underbrace{\begin{bmatrix} \Delta x(k) \\ y(k) \end{bmatrix}}_{x(k)} \end{aligned} \tag{5}$$

where k is the current sample time, $\Delta x(k+1) = x(k+1) - x(k)$, $\Delta x(k) = x(k) - x(k-1)$, $\Delta u(k) = u(k) - u(k-1)$, O denotes a zero matrix with dimensions indicated by subscripts. n_x and p_y represent the state and output dimensions, respectively, while $\{A, B, C\}$ defines the state-space model.

Define $Y = [y(k+1), y(k+2), \cdots, y(k+n_y)]^T$ and $\Delta U = [\Delta u(k), \Delta u(k+1), \cdots, \Delta u(k+n_u-1)]^T$, we can get $Y = Px(k) + H\Delta U$ with $P = [CA, CA^2, CA^3, \cdots, CA^{n_y}]^T$ and $H = [CB, 0, \cdots, 0; CAB, CB, \cdots, 0; CA^2B, CAB, \cdots, 0; \cdots; CA^{n_y-1}B, CA^{n_y-2}B, \cdots, CA^{n_y-n_u}B]$ where n_u and n_y are the control and prediction horizons, respectively, satisfying $n_u \le n_y$. Constraints on $u(k)$ and $\Delta u(k)$ ensure the system remains within a safe and feasible range: $D\Delta U \le dd$, where $D = [-D_1, D_1, -E, E]^T$ and $dd = [-U^{min} + D_2u(k-1), U^{max} - D_2u(k-1), -\Delta U^{min}, \Delta U^{max}]^T$ with U^{min} and U^{max} are respectively the maximum and minimum sequence of $\Delta u(k)$, $D_1 = [E, 0, 0, \cdots, 0; E, E, 0, \cdots, 0; \cdots; E, E, E, \cdots, E]$, and $D_2 = [E, E, \cdots, E]^T$. The controller computes the optimal control inputs at each sampling instant by minimizing the error between the predicted and the desired outputs. This optimization objective is formulated as

$$J = \frac{1}{2}\Delta U^T M \Delta U + \Delta U^T F \tag{6}$$

where $M = 2(H^TH + K)$, with K being the diagonal weight matrix for the control input, and $F = -2H^T(R_s - Px(k))$, where $R_s = [E, E, \cdots, E]^T r(k)$, with $r(k)$ denoting the desired reference at time k. Both M and F are compatible matrices in the quadratic programming formulation.

D. Differential Flatness

Differential flatness has been extensively utilized in quadrotor trajectory generation and optimization, as it significantly reduces the dimensionality and complexity of planning and control problems [7]. The morphing quadrotor system also has the property of differential flatness. By selecting appropriate flat output variables, all system states $x = [x, y, z, \phi, \theta, \psi, \dot{x}, \dot{y}, \dot{z}, p, q, r, \ell]^T$ and control inputs u can be represented as algebraic functions of the flat outputs and a finite number of their derivatives.

Using differential flatness mappings Ψ_x and Ψ_u, $x(t)$ and $u(t)$ can be expressed in terms of flat output $\xi(t)$ as

$$\begin{aligned} x(t) &= \Psi_x(\xi(t), \dot{\xi}(t), \ldots, \xi^{(s-1)}(t)) = \Psi_x(\xi^{[s-1]}(t)) \\ u(t) &= \Psi_u(\xi(t), \dot{\xi}(t), \ldots, \xi^{(s)}(t)) = \Psi_u(\xi^{[s]}(t)) \end{aligned} \tag{7}$$

where s denotes the order of the polynomial derivatives. Then, the constraint $h(x,u)$, which depends on the system states and control inputs, can be reformulated in terms of the flat outputs as

$$h(\Psi_x(\xi^{[s-1]}(t)),\ \Psi_u(\xi^{[s]}(t))) = h_\Psi(\xi^{[s]}(t)) \tag{8}$$

which provides support for the trajectory optimization algorithm in Section III, enabling the conversion of the planning problem under complex dynamic constraints into a convex optimization problem in the flat space.

III. Time-Optimal Based Trajectory Generation

In this section, we systematically address the waypoint-based spatial constraints of the morphing quadrotor and eliminate them through parameterization. Then, we formulate a time-optimal waypoint traversal problem, after which we employ a polynomial trajectory representation and further

reformulate the constrained problem into an unconstrained optimization problem.

A. Definition of Waypoint

In trajectory planning tasks, the quadrotor starts from a given initial position, passes n waypoints in sequence, and finally reaches the end point. The region associated with the i-th waypoint region is denoted as

$$\mathcal{P}_i = \left\{ p_i \in \mathbb{R}^3 \middle| \|p_i - o_i\|_2 \leq \delta_i - \ell_i, i = 1,2,\ldots,n \right\} \tag{9}$$

where o_i denotes the center position of the i-th waypoint, p_i represents the quadrotor's actual position at traversal, δ_i indicates the radius of the region, and ℓ_i corresponds to the arm length of the quadrotor at the waypoint. The above set-based condition ensures that the morphing quadrotor remains within a safe and feasible domain during traversal, preventing any part of the body from exceeding boundaries. To formalize this safety requirement, we define a constraint function in the form of $h_{\mathcal{P}_i}(p_i) \leq 0$.

B. Position Constraint Elimination

Conventional methods typically impose the position constraint $h_{\mathcal{P}_i}(p_i) \leq 0$ directly into the optimization problem, introducing a large number of Lagrange multipliers and thus degrading both convergence speed and numerical stability. To address this, a variable substitution strategy was proposed in [20], where a smooth mapping $f_B(q,\ell)$ transforms an unconstrained variable q into p that inherently satisfies the constraint, eliminating explicit inequality constraints and simplifying optimization. The mapping is defined as

$$f_B(q,\ell) = o + \frac{2(\delta - \ell)q}{q^T q + 1} \tag{10}$$

Because ℓ is variable, the bounded constraint $\delta - \ell \in [r_{min}, r_{max}]$ is enforced by introducing an unconstrained variable s and applying a sigmoid-based transformation. The final mapping is defined as

$$f_{B'}(q,s) = o + \frac{2q}{q^T q + 1}\left(r_{min} + \frac{r_{max} - r_{min}}{1 + e^{-s}}\right) \tag{11}$$

By parameterizing p and ℓ in terms of q and s, the positional constraints on the trajectory are successfully eliminated, which will be leveraged later.

C. Problem Formulation

The system dynamics are described by the differential equation $\dot{x} = f(x,u)$, and are subject to a set of state-control inequality constraints $h(x,u) \leq 0$. Then the time-optimal trajectory planning problem can be formulated as

$$\min_{x,u,t_k} \quad \int_0^{t_k} 1\, dt \tag{12a}$$

$$\text{s.t.} \quad h_{\mathcal{P}_i}(p_{x(t_i)}) \leq 0, \quad 1 \leq i \leq n, \tag{12b}$$

$$x(0) = \bar{x}_{init},\ x(t_k) = \bar{x}_k, \tag{12c}$$

$$\dot{x} = f(x,u),\ h(x,u) \leq 0, \tag{12d}$$

where t_i is the time at which the trajectory passes through the i-th waypoint, and $p_{x(t_i)}$ represents the position component of the state vector $x(t_i)$. The initial and end states are denoted by $\bar{x}_{init}$ and $\bar{x}_k$, respectively.

Due to the system's differential flatness, both x and u can be uniquely represented by (8). Consequently, (12) can be reformulated in the flat space

$$\min_{\xi,t_k} \quad \int_0^{t_k} 1\, dt \tag{13a}$$

$$\text{s.t.} \quad h_{\mathcal{P}_i}(p_{x(t_i)}) \leq 0, \quad 1 \leq i \leq n, \tag{13b}$$

$$\xi^{[s-1]}(0) = \bar{\xi}^{[s-1]}_{t_{init}}, \tag{13c}$$

$$\xi^{[s-1]}(t_k) = \bar{\xi}^{[s-1]}_{t_k}, \tag{13d}$$

$$h_\Psi(\xi^{[s]}) \leq 0. \tag{13e}$$

But there are two main challenges in the above optimization formulation: The constraint $h_{\mathcal{P}_i}(p_{x(t_i)}) \leq 0$ explicitly depends on the time variable t_i, introducing a directly coupling between position and time; The infinite-dimensional property of the continuous trajectory $\xi(t)$ increases the complexity of the direct solution. Therefore, it is necessary to appropriately reformulate this constraint in order to decouple the time variable from the position constraint.

To this end, the entire trajectory is divided into $n+1$ segments by n waypoints, denoted as $P = [p_1^T, p_2^T, \ldots, p_n^T]^T$. The corresponding segment durations are $T = [T_1, T_2, \ldots, T_{n+1}]^T$ with total duration $t_k = T_\Sigma$ and cumulative time $t_i = \sum_{j=1}^{i} T_j$. Therefore, the position of the trajectory at time t_i is defined to be that of the i-th waypoint as $p_{x_{t_i}} = p_i$.

Additionally, we define

$$\mathfrak{T}(P) = \left\{ T \in \mathbb{R}_{>0} \middle| \begin{array}{l} \exists\, \xi : [0, T_\Sigma] \to \mathbb{R}^n \text{ such that} \\ \quad \xi^{[s-1]}(0) = \xi^{[s-1]}_{\text{init}}, \\ \quad \xi^{[s-1]}(t_k) = \xi^{[s-1]}_{t_k}, \\ \quad h_\Psi(\xi^{[s]}(t)) \leq 0, \quad \forall t \in [0, t_k], \\ \quad p_x(t_i) = p_i, \quad 1 \leq i \leq n \end{array} \right\}$$

as the set of all dynamically feasible time allocations satisfying the prescribed constraints, with an associated indicator function

$$\rho_{\mathfrak{T}(P)}(T) = \begin{cases} 0, & \text{if } T \in \mathfrak{T}(P), \\ \infty, & \text{otherwise.} \end{cases} \tag{14}$$

to ensure that a given time allocation satisfies the aforementioned trajectory feasibility conditions, whose detailed explanation is provided in the following subsection.

D. Reformulation of Polynomial Trajectory Optimization

$\mathfrak{T}(P)$ describes all possible time allocations that satisfy dynamic feasibility, trajectory continuity, and waypoint constraints. However, directly handling the indicator function $\rho_{\mathfrak{T}(P)}(T)$ and the set $\mathfrak{T}(P)$ is computationally complex and analytically intractable. Thus, we utilize the Minimum Control (MINCO) [20] trajectory representation as a foundational framework to generate analytically structured and dynamically feasible trajectories.

MINCO formulates trajectory generation as a multi-segment polynomial optimization minimizing control effort under boundary derivative constraints, providing a

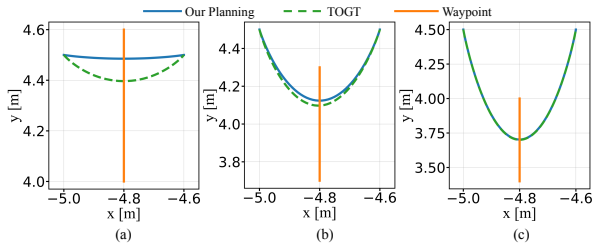

Fig. 2. Top-down view of the trajectories generated by our method (blue solid line) and the TOGT method (green dashed line). Orange segments represent the required waypoints. The positions of initial and end points are $(-5.0, 4.5, 1.2)$ and $(-4.6, 4.5, 1.2)$. The waypoints for the three experiments are located at $(-4.6, 4.3, 1.2)$, $(-4.6, 4.0, 1.2)$, and $(-4.6, 3.7, 1.2)$, respectively, each with a radius of 0.3 m.

unified spatiotemporal representation that ensures continuity and smooth dynamics. Unlike traditional splines, MINCO enables closed-form control inputs computation and continuous-time constraints. Thus, we redefine the trajectory feasibility set $\mathfrak{T}(P)$ using the MINCO representation $\rho_{\mathfrak{T}(P)}(T) = \int_0^{T_\Sigma} \max[h_\Psi(\xi^{[s]}), 0]^k dt$ which is approximated using numerical sampling as

$$\rho_{\mathfrak{T}(P)}(T) \approx \sum_{i=1}^{M} \frac{T_i}{\kappa_i} \sum_{j=0}^{\kappa_i} \gamma_j \max[h_\tau(T_i, \tfrac{j}{\kappa_i}), 0]^k \tag{15}$$

where κ_i is the number of samples for segment, γ_j represents the corresponding quadrature weights, and $h_\tau(T_i, \tau) = h_\Psi(\xi^{[s]}(\tau T_i))$ denotes the evaluation of the constraint at a discrete time. Then, the trajectory optimization problem is formulated as

$$\min_{P,T} \quad T_\Sigma + \rho_{\mathfrak{T}(P)}(T) \tag{16a}$$

$$\text{s.t.} \quad h_{\mathcal{P}_i}(p_i) \le 0, \quad 1 \le i \le n \tag{16b}$$

E. Unconstrained Optimization

At this stage, only P and T remain as the optimization variables. By applying the transformation in (11), P is reformulated using the unconstrained variables $Q = \left[q_1^T, q_2^T, \ldots, q_n^T\right]^T$ and $S = [s_1, s_2, \ldots, s_n]^T$. Similarly, to ensure non-negativity, T is parameterized by an unconstrained variable $K = [k_1, k_2, \ldots, k_n, k_{n+1}]^T$. This reformulation converted the problem into an unconstrained optimization

$$\min_{Q,S,K} \quad T_\Sigma(K) + \rho_{T(Q,S)}(K) \tag{17}$$

In this way, the problem is efficiently computed with the optimal values of Q, S, and K. Subsequently, the original variables P, ℓ, and T are recovered through the corresponding mappings. These are then used to construct the time-parameterized polynomial trajectories of P and ℓ for execution by the controller.

IV. EXPERIMENTS

In this section, we evaluate the performance of the proposed trajectory planning and control framework through a series of experiments. We first conduct comparative tests in less challenging environments to validate the effectiveness of our method in improving trajectory efficiency through structural adaptation. Next, a challenging seven-stage morphing experiment demonstrates the planner's capability to generate feasible and efficient trajectories when flying through a series of different circular apertures. Finally, we implement an MPC-based controller for trajectory tracking to assess the feasibility and accuracy of the planned trajectories under dual-loop control.

A. Evaluation in Single-Stage Radius Transition

To validate the effectiveness of our proposed time-optimal trajectory planning method that accounts for variations in the quadrotor arm length, we conducted three sets of comparative experiments using simplified scenarios in Fig. 2. These experiments aim to validate our method's adaptability and generality across diverse waypoint constraints. In each experiment, the quadrotor flew from the same initial point to the same end point, sequentially passing through different circular waypoints while ensuring collision avoidance and optimizing the trajectory for minimum completion time by considering the arm length. Our method is compared against the TOGT [9] approach from two dimensions: path length and flight time. The results demonstrate that our approach achieved reductions in path length by 14.39%, 5.08%, and 0.2%, and reductions in flight time by 19.77%, 2.23%, and 0.08% across the three scenarios, respectively. Although the performance gains decrease as the overall path length increases, our method consistently outperforms the TOGT approach. These results highlight the potential of incorporating structural variability to enhance trajectory-planning performance, particularly for dynamic tasks that require tight obstacle traversal or rapid response.

B. Trajectory Generation with 7-Stage Radius Transitions

The previous experiments have demonstrated the effectiveness of the proposed method. To further evaluate its performance under complex and constrained environments, we construct a flight scenario consisting of seven different waypoints which is designed with reference to the flight environment described in [21], simulating a challenging task, where the quadrotor must traverse a sequence of progressively narrowing spaces. The planned trajectory generated by our method is shown as a light blue curve, the waypoints are represented as orange circles, while the quadrotor is visualized as a black "×" symbol, with its arm length represented by the size of the cross in Fig. 3. The trajectory requires the quadrotor to pass through increasingly narrow gaps, necessitating continuous adaptation of the arm length. In the zoomed-in plot around p_3 in Fig. 3(a), it can be observed that the quadrotor proactively adjusts its arm length before entering the constrained area, enabling it to pass safely and smoothly without collisions. In the zoomed-in plots in Fig. 3(b), from p_1 to p_7, the arm length gradually contracts in response to the shrinking radius sizes of the waypoints. By the time the quadrotor reaches end position, the arm length has been reduced from its initial maximum value

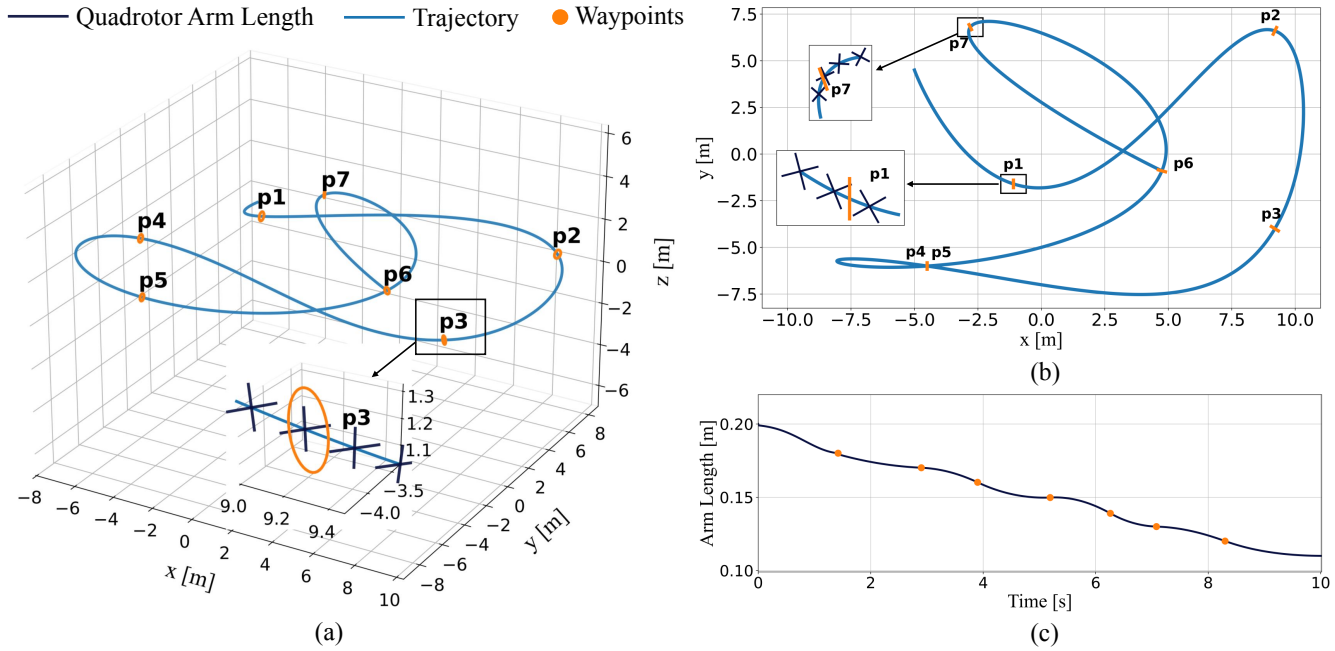

Fig. 3. Trajectory generation of the morphing quadrotor with seven-stage radius variation: (a) 3D trajectory, (b) top view, and (c) arm length variation over time. (a) and (b) are partially enlarged. The waypoints are centered at $p_1 = (-1.1, -1.6, 3.6)$, $p_2 = (9.2, 6.6, 1.0)$, $p_3 = (9.2, -4.0, 1.2)$, $p_4 = (-4.5, -6.0, 3.5)$, $p_5 = (-4.5, -6.0, 0.8)$, $p_6 = (4.75, -0.9, 1.2)$, and $p_7 = (-2.8, 6.8, 1.2)$, with radius gradually decreasing 0.01 m from 0.19 m to 0.13 m, forming a seven-stage narrowing corridor. The initial and end positions are set to $(-5.0, 4.5, 1.2)$ and $(4.75, -0.9, 1.2)$, respectively.

$\ell_{\max} = 0.2$ m to a minimum value $\ell_{\min} = 0.11$ m as shown in Fig. 3(c).

During this process, a time-optimal trajectory of total length 92.2068 m is successfully generated, and the entire flight task is completed within 10.0168 s. The quadrotor maintains safe and stable flight, demonstrating the system's capability to ensure dynamic feasibility and robust performance in constrained environments. The results validate that the proposed time-optimal trajectory generation framework can produce smooth and feasible flight paths under multiple constraints by incorporating arm length variation as an optimization variable, while minimizing the flight duration. Ultimately, we obtain time-parametrized polynomial trajectories for position and arm length $[x_d(t), y_d(t), z_d(t), \ell_d(t)]$, which serve as reference inputs for the downstream control module, ensuring the quadrotor executes missions efficiently and safely.

C. MPC-based Trajectory Tracking

To achieve high-precision tracking, a full-DOF dual-loop enhanced controller based on MPC was implemented. The key parameters include $m = 0.85$ kg, $g = 9.81$ m/s^2, and attitude angles $\phi, \theta \in [-\pi/5, \pi/5]$ rad with $\psi = 0$ rad. The total thrust T is constrained within $[-mg, mg]$. To meet system dynamic constraints, the variations in attitude angles $\Delta\phi, \Delta\theta$ and thrust ΔT are limited to $\pm 60\%$ of their respective maximum values. Furthermore, rotor speeds are constrained between 3093 rpm and 4720 rpm to reflect the physical limitations of the motors. In MPC design, the prediction horizon N_Y and control horizon N_U for the outer loop are set to 20 and 3, respectively. During the test process,

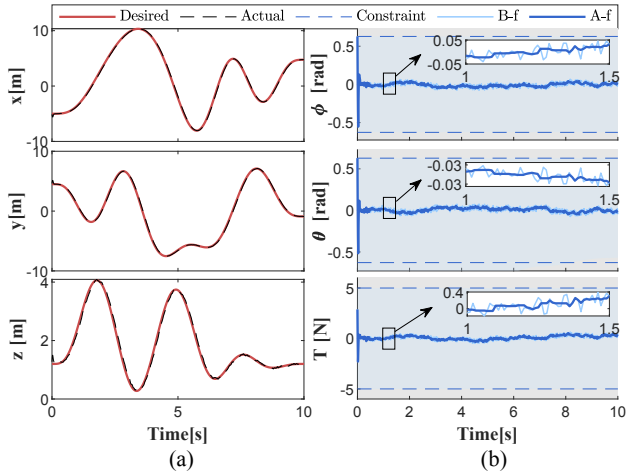

Fig. 4. Results of the MPC position controller: (a) position tracking performance and (b) control inputs subject to constraints, with selected segments enlarged for detailed visualization. B-f represents the unfiltered curve, while A-f denotes the curve after filtering.

a random disturbance with amplitude $0.01 \times \text{rand}(1)$ was embedded into the dynamic model to verify the robustness. Fig. 4 and Fig. 5 illustrate the position and attitude tracking performance of the proposed controller. Specifically, the desired trajectory generated by the time-optimal planning module is shown as red solid lines, and the desired attitude generated by the outer loop is shown as blue solid lines, while the actual position and attitude are all depicted with black dashed lines. In all spatial and attitude dimensions, the controller rapidly converges to the desired reference despite

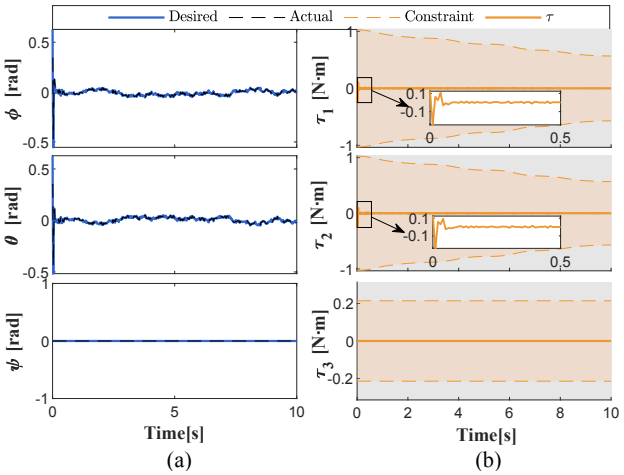

Fig. 5. Results of the MPC position controller: (a) attitude tracking performance and (b) control inputs subject to constraints, with selected segments enlarged for detailed visualization.

minor initial deviations, achieving high-accuracy tracking in the presence of random disturbances. For the outputs, ϕ, θ, and T are shown as light blue solid lines, which are processed using median filtering to suppress high-frequency oscillations, thereby yielding smooth control signals without abrupt changes, shown as dark blue solid lines. The generated control torques are shown as orange solid lines. All outputs remain within the dashed-line constraints, and their rates of change also satisfy the limits. The inner loop constraints are dynamically adjusted over time to reflect structural morphing as the arm length varies. Therefore, the MPC-based dual-loop enhanced controller demonstrates high accuracy and stability in tracking spatial trajectories and attitude dynamics. It exhibits rapid convergence even in the presence of external disturbances and initial deviations, validating the controller's superior performance and robustness during complex, continuous morphing quadrotor maneuvers.

V. CONCLUSIONS

We present a time-optimal trajectory planning and dual-loop control framework for the morphing quadrotor. Unlike existing methods, it explicitly integrates arm length variations into flight dynamics. In the trajectory generation phase, the dynamic adjustment of arm length allows the quadrotor to navigate through narrow and constrained waypoints that are typically unreachable for rigid-body quadrotors. On the control side, a full-DOF dual-loop enhanced controller based on MPC is proposed, whose outer loop ensures accurate tracking of the reference position trajectory, while the inner loop concurrently regulates both the attitude and arm length. Experimental results validate the effectiveness of the proposed framework, demonstrating superior trajectory feasibility, control precision, and dynamic responsiveness in complex environments.

REFERENCES

[1] H. Yu, X. Liang, J. Han, and Y. Fang, "Adaptive trajectory tracking control for the quadrotor aerial transportation system landing a payload onto the mobile platform," *IEEE Transactions on Industrial Informatics*, vol. 20, no. 1, pp. 23–37, 2023.

[2] N. Bucki, J. Tang, and M. W. Mueller, "Design and control of a midair-reconfigurable quadcopter using unactuated hinges," *IEEE Transactions on Robotics*, vol. 39, no. 1, pp. 539–557, 2022.

[3] D. Falanga, K. Kleber, S. Mintchev, D. Floreano, and D. Scaramuzza, "The foldable drone: A morphing quadrotor that can squeeze and fly," *IEEE Robotics and Automation Letters*, vol. 4, no. 2, pp. 209–216, 2018.

[4] P. Foehn, A. Romero, and D. Scaramuzza, "Time-optimal planning for quadrotor waypoint flight," *Science Robotics*, vol. 6, no. 56, p. eabh1221, 2021.

[5] A. Romero, S. Sun, P. Foehn, and D. Scaramuzza, "Model predictive contouring control for time-optimal quadrotor flight," *IEEE Transactions on Robotics*, vol. 38, no. 6, pp. 3340–3356, 2022.

[6] Z. Zhou, G. Wang, J. Sun, J. Wang, and J. Chen, "Efficient and robust time-optimal trajectory planning and control for agile quadrotor flight," *IEEE Robotics and Automation Letters*, vol. 8, no. 12, pp. 7913–7920, 2023.

[7] D. Mellinger and V. Kumar, "Minimum snap trajectory generation and control for quadrotors," in *2011 IEEE International Conference on Robotics and Automation (ICRA)*, pp. 2520–2525, IEEE, 2011.

[8] D. Mellinger, N. Michael, and V. Kumar, "Trajectory generation and control for precise aggressive maneuvers with quadrotors," *The International Journal of Robotics Research*, vol. 31, no. 5, pp. 664–674, 2012.

[9] C. Qin, M. S. Michet, J. Chen, and H. H.-T. Liu, "Time-optimal gate-traversing planner for autonomous drone racing," in *2024 IEEE International Conference on Robotics and Automation (ICRA)*, pp. 8693–8699, IEEE, 2024.

[10] Y. Xin, X. Lu, and F. Li, "Simulation research on time-optimal path planning of uav utilizing the flightmare platform," in *2024 14th International Conference on Information Science and Technology (ICIST)*, pp. 784–790, 2024.

[11] C. Qin, J. Chen, Y. Lin, A. Goudar, A. P. Schoellig, and H. H.-T. Liu, "Time-optimal planning for long-range quadrotor flights: An automatic optimal synthesis approach," *arXiv preprint arXiv:2407.17944*, 2024.

[12] N. Zhao, W. Yang, C. Peng, G. Wang, and Y. Shen, "Comparative validation study on bioinspired morphology-adaptation flight performance of a morphing quad-rotor," *IEEE Robotics and Automation Letters*, vol. 6, no. 3, pp. 5145–5152, 2021.

[13] G. Cui, R. Xia, X. Jin, and Y. Tang, "Motion planning and control of a morphing quadrotor in restricted scenarios," *IEEE Robotics and Automation Letters*, vol. 9, no. 6, pp. 5759–5766, 2024.

[14] Y. Wu, F. Yang, Z. Wang, K. Wang, Y. Cao, C. Xu, and F. Gao, "Ring-rotor: A novel retractable ring-shaped quadrotor with aerial grasping and transportation capability," *IEEE Robotics and Automation Letters*, vol. 8, no. 4, pp. 2126–2133, 2023.

[15] M. Xu, Q. De, D. Yu, A. Hu, Z. Liu, and H. Wang, "Biomimetic morphing quadrotor inspired by eagle claw for dynamic grasping," *IEEE Transactions on Robotics*, vol. 40, pp. 2513–2528, 2024.

[16] K. Patnaik and W. Zhang, "Adaptive attitude control for foldable quadrotors," *IEEE Control Systems Letters*, vol. 7, pp. 1291–1296, 2023.

[17] T. Yang, Y. Zhang, P. Li, Y. Shen, Y. Liu, and H. Chen, "Sniae-sse deformation mechanism enabled scalable multicopter: Design, modeling and flight performance validation," in *2020 IEEE International Conference on Robotics and Automation (ICRA)*, pp. 864–870, IEEE, 2020.

[18] C. Qin, N. Zhao, Q. Wang, Y. Luo, and Y. Shen, "Minimum snap trajectory planning and augmented mpc for morphing quadrotor navigation in confined spaces," *Drones*, vol. 9, no. 4, p. 304, 2025.

[19] N. Zhao, Y. Luo, C. Qin, X. Luo, R. Chen, and Y. Shen, "Attitude control for morphing quadrotor through model predictive control with constraints*," in *2024 IEEE International Conference on Robotics and Automation (ICRA)*, pp. 10489–10495, 2024.

[20] Z. Wang, X. Zhou, C. Xu, and F. Gao, "Geometrically constrained trajectory optimization for multicopters," *IEEE Transactions on Robotics*, vol. 38, no. 5, pp. 3259–3278, 2022.

[21] S. Sun, A. Romero, P. Foehn, E. Kaufmann, and D. Scaramuzza, "A comparative study of nonlinear mpc and differential-flatness-based control for quadrotor agile flight," *IEEE Transactions on Robotics*, vol. 38, no. 6, pp. 3357–3373, 2022.